Microsyst Technol (2007) 13:1241–1252
DOI 10.1007/s00542-006-0336-3

TECHNICAL PAPER

Dynamical modeling and experimental validation of a micro-speaker with corrugated diaphragm for mobile phones

Paul C.-P. Chao · I-Ting Wang

Received: 30 June 2006 / Accepted: 15 November 2006 / Published online: 14 December 2006

Abstract As the design trend of modern cellular phones evolves to be miniaturization and versatile sound in quality, the electro-mechanical components including the micro-speaker are essential toward size reduction and broad frequency range of sound. To reduce size, a diaphragm type micro-speaker is commonly employed in industry, while to broaden the sound frequency range corrugations on the diaphragm are adopted. The corrugations are generally capable of leading to fairly flat response over a broad range since diaphragm stiffness is decreased in axial direction. To confirm the aforementioned capability, the modeling on a corrugated diaphragm is performed first using finite element method (FEM) to obtain the associated dynamic equations in terms of modal coordinates; then the equations are next combined with the magneto-electrical model of the voice coil motor (VCM) that is attached to the bottom side of the diaphragm. Finally, the acoustic effects of the air inertia on the diaphragm and vents of the outer case are modeled using basic acoustic theories. Assembling all derived system equations and solving them, the frequency response of the micro-speaker in sound pressure level (SPL) can be simulated. It shows that the diaphragm corrugation in fact helps flatten the SPL response of the micro-speaker (especially in high frequency range) to lessen sound distortion. Furthermore, the corrugation angle approximately below 45° is favored over other angles or flatter SPL response. Experiments are also conducted to verify the theoretical findings.

P. C.-P. Chao (✉)
Department of Electrical and Control Engineering,
National Chiao Tung University,
Hsinchu 3200, Taiwan, ROC
e-mail: pchao@mail.nctu.edu.tw

I-T. Wang
Department of Mechanical Engineering,
R&D Center for Membrane Technology,
Chung-Yuan Christian University,
Chung-Li 32023, Taiwan, ROC

1 Introduction

In response to recent demands for miniaturization and high sound quality of commercial cell phones, the micro-speaker employed in mobile phones is expected to have a significant reduction in size and also provides a broad frequency range of realistic sound responses. Toward the aforementioned end, a micro-speaker with a vibrating diaphragm responsible for generating sound are commonly employed. A schematic of the micro-speaker is shown in Fig. 1, which consists mainly of the diaphragm and the voice coil motor (VCM) attached at the bottom of the diaphragm. The VCM is movable between the top plate and the U-yoke. Having applied voltage to the VCM, the electro-magnetic interaction between the magnetic field and the VCM current would produce electromagnetic forces to drive the diaphragm to vibrate and then generate sound.

Conventional macro-sized loudspeakers were fully investigated and applied to a mature stage. Earlier works dedicated to the modeling on conventional loudspeakers with or without enclosures such as sealed and vented ones adopted the technique of lumped-parameter modeling, which provides a quick analysis and satisfactory accuracy at low frequencies (Beranek

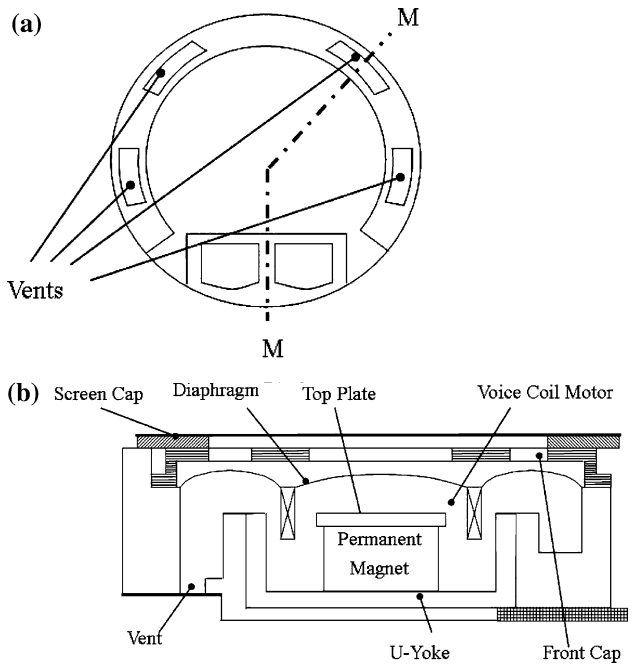

Fig. 1 Schematic of the moving-coil type micro-speaker. **a** Bottom view, **b** M–M cross-sectional view

1954; Small 1972; Small 1972; Novak 1959; Tappan 1959). In addition, some works were focused on the nonlinear effects of the loudspeakers like uneven magnetic flux distribution on the micro-speaker dynamics (Al-Ali et al. 2000; Kaizer 1987; Kippel 1990, 1992). However, as the commercial demand increases for small-sized speakers, as used in cell phones, the lumped-model is not sufficient to accurately predict the speaker performance at high frequencies, which becomes much more important information for mobile phone designs nowadays. The approach adopting a distributed parameter model, like the finite element analysis (FEA), was then required. Hwang et al. (2002a) conducted a FEA modeling on the vibrating diaphragm, along with consideration of the magneto-electro-mechanical coupling effects between vibrating diaphragm, coils and the magnetic flux induced by the surrounding magnets. Recently, researchers continued to dedicate their efforts to perform the dynamic modeling with special regards for effects of uneven magnetic fields (Hwang et al. 2002b), various shapes of the diaphragm (Hwang et al. 2003a) and optimum placement of the magnets(Hwang et al. 2003b).

The aforementioned studies, however, lack consideration of commonly-seen diaphragm corrugations as shown in Fig. 2. The corrugations are in fact employed in most of commercialized mobile speakers to enhance high-frequency sensitivities to required levels. In this way, a fairly flat frequency response over a broad range can be achieved to avoid sound distortion to human ears. With the main goal of confirming the effectiveness and distilling design guidelines of the corrugation, theoretical and experimental studies are conducted in this study. The theoretical study starts with performing finite element modeling on the corrugated diaphragm, in which process various cut angles of diagram corrugations are considered. The obtained finite element model is further reduced to limited number of modes up to 20 kHz, the upper limit of human audibility. These modes are then combined with the magneto-electrical model of the voice coil motor (VCM) in the micro-speaker. The driving force generated the VCM for the diaphragm to vibrate is carried out based on another group of finite elements for modeling the magnetic field around the VCM. Finally, to seek more precise modeling, the acoustic effects of the air inertia in front of the diaphragm and in the vents are further modeled using the theory of radiation and effective masses. Assembling all derived sub-system equations and solving them, the frequency responses of a micro-speaker can be obtained. Besides the theoretical study, an experiment system is also designed and used to measure the sound pressure level (SPL) of the micro-speaker. The obtained experimental SPLs as opposed to varied frequency are compared with their simulated counterparts. A general closeness is found between them, showing the effectiveness of the theoretical model established and the subsequent designs.

The paper is organized as follows. In Sect. 2, the mathematical model consisting of mechanical, electrical and magnetic subsystems is established. In Sect. 3, simulations are conducted. Section 4 presents experimental study. Section 5 provides conclusions.

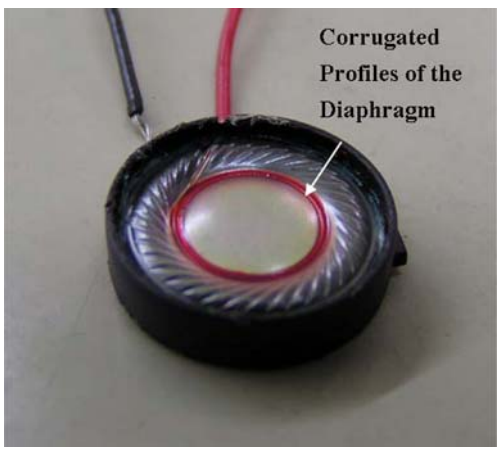

Fig. 2 Corrugated profiles of the diaphragm in the micro-speaker

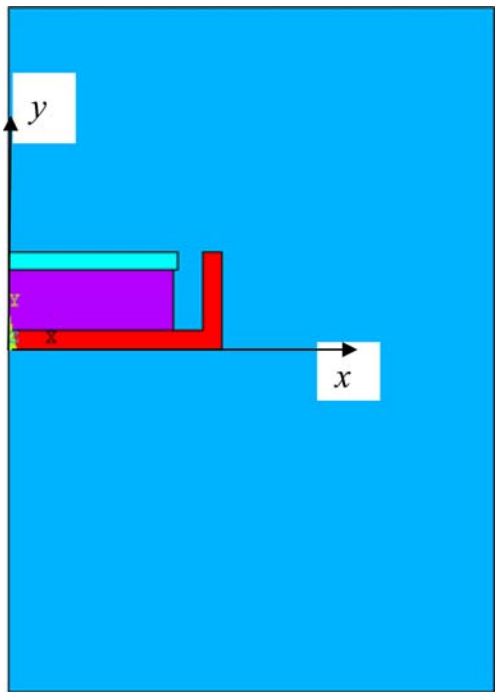

Fig. 3 The 2D axisymmetric magnetic system of the micro-speaker

2 Mathematical modeling

This section presents electromagnetic, mechanical, and acoustical modeling for the respective subsystems in a micro-speaker. Nonlinear effects of uneven magnetic flux distribution are taken into accounts in the electromagnetic analysis. In order to incorporate corrugated profiles of the diaphragm, finite element method (FEM) and modal analysis are adopted. Finally, to put emphases on the high-frequency responses of the micro-speaker, acoustical effects of the radiation mass, and effective mass of the vents are considered. The dynamic performance of the micro-speaker can then be obtained and assessed.

2.1 Electromagnetic modeling

The electromagnetic system of the micro-speaker, as shown schematically in Fig. 1, is composed of a voice coil motor (VCM), a top plate, a permanent magnet, and a U-yoke. With a voltage applied to VCM, the current in VCM is generated to move through the magnetic field. The interaction between the current in the VCM and the magnetic field results in an axial Lorentz force, which can be expressed as Equation-Equation

$$F = \oint I \mathrm{d}l \times B, \tag{1}$$

where B, l, and I represent magnetic flux intensity, the wire length of the VCM, and the current in VCM, respectively. The magnetic flux intensity B in the micro-speaker would be solved based on Maxwell's equations, which is in this study realized by finite elements modeling via the software ANSYS. Prior to solving for B, some assumptions are made. First, the magnetic flux distribution in the micro-speaker, B, is assumed static such that the effect of the current back on the magnetic field is not considered. Second, due to the fact that the magnetic system of the micro-speaker is in an annular axisymmetric structure, the magnetic system can well be considered as a 2D axisymmetric model, as shown in Fig. 3 Third, in order to realize the condition of open-space-like enclosure around the magnet, boundary conditions are set to constrain magnetic flux as parallel to the air boundaries of the FEM model around the magnetic system as shown in Fig. 3. The related material properties of the components of the magnetic system are listed in Table 1. Figure 4 presents the magnetic flux intensity distribution resulted from ANSYS modeling and simulations. It can be observed from this figure that the magnetic flux intensity is concentrated in the air gap between the top plate and its facing U-Yoke surface, as the result of magnetic flux being guided from the permanent magnet to the yoke through the air gap. Extracting calculated magnetic flux intensities vertically along the gap centerline from finite element simulated results and then employing a polynomial to fit the varied flux intensity yield

$$B(y_v) = a_4 y_v^4 + a_3 y_v^3 + a_2 y_v^2 + a_1 y_v + a_0, \tag{2}$$

where $B(y_v)$ is a fourth-order polynomial of the vertical (axial) displacement of the VCM coils, y_v. The coefficients a's can be obtained as shown in Table 2 after a curve-fitting is performed. With the expression of B in Eq. 2 in hand, the next step is to derive the current in VCM, which can be determined from the electric equilibrium in the entire set of VCM, yielding

Table 1 Material properties of the components of the magnetic filed

Components	Properties		
	Air	Permanent magnet	Top plate and U-yoke
Relative permeability	1	1.27	2,000
Coercive force (A/m)	–	9.15×10^5	–

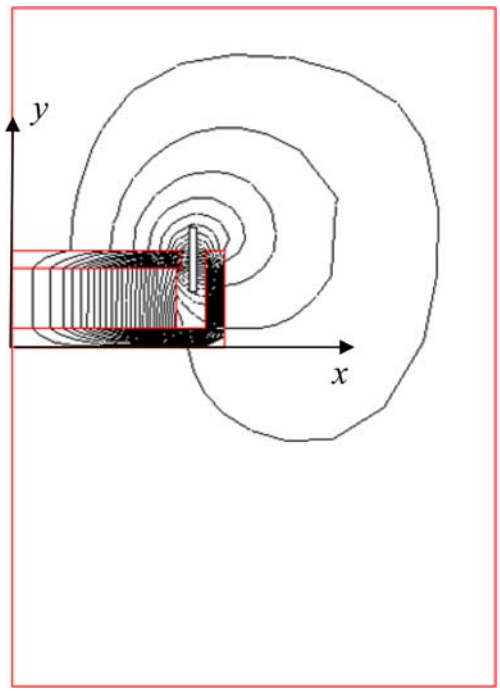

Fig. 4 The magnetic flux distribution in the micro-speaker

Table 2 Solved coefficients a's of the fourth-order polynomial $B(y_v)$

a_4 (T/m^4)	a_3 (T/m^3)	a_2 (T/m^2)	a_1 (T/m)	a_0 (T)
9.4257×10^{11}	8.6203×10^7	-7.4671×10^5	–54.928	0.24951

$$V = RI + L\frac{\mathrm{d}I}{\mathrm{d}t} + B(y_v)l\dot{y}_v, \tag{3}$$

where V, R, L, and $\dot{y}_v$ denote the applied voltage, the resistance, the inductance, and the axial velocity of the VCM, respectively. Note that the last term in Eq. 3 results from the back electromotive force (EMF) which is caused by the interaction between the current and the magnetic field.

2.2 Mechanical modeling

Considering geometry complexity evolved in the vibrating corrugated diaphragm, method of finite element modeling (FEM) is adopted for subsequent mechanical vibration analysis. Using the meshing tool provided by ANSYS, a relative complicated finite element model is established, where shell elements are utilized for both the diaphragm and VCM. The material properties for a practical micro-speaker, as photo-shown in Fig. 2, are given in Table 3 for this study. Figure 5 shows the established model from various points of view, where the corrugation has a baseline 45° with respect to the radial direction as shown in the figure. With the finite element model built, the mechanical equations of motion of the diaphragm and the VCM can then be extracted from the meshed model in compact matrix form as

$$\mathbf{M}\ddot{\mathbf{y}} + \mathbf{C}\dot{\mathbf{y}} + \mathbf{K}\mathbf{y} = \mathbf{f}, \tag{4}$$

where **M, C, K**, and **f** denote a mass matrix, a damping matrix, a stiffness matrix of the vibration system, and an axial force vector exerted by the VCM, respectively. The axial force **f** owns non-zero components corresponding to the axial direction and at the nodes along the circumference of the VCM coils. Each of the non-zero components is obtained with distributing the bulk Lorentz force F in Eq. 1 evenly along the VCM circumference. On the other hand, the mass and stiffness matrices are derived by the finite elements established by ANSYS. As to the damping matrix **C**, it can reasonably be assumed to be a liner combination of mass and stiffness based on basic theory of vibration (Rao 1990), which is in the form of

$$\mathbf{C} = \alpha\mathbf{M} + \beta\mathbf{K}, \tag{5}$$

where α and β are constants to be further determined. For the current case, it can be assumed the higher modes are slightly damped; thus, $\beta = 0$. The damping matrix in Eq. 5 can be consequently expressed as

$$\mathbf{C} = \alpha\mathbf{M}. \tag{6}$$

Having successfully established the equations of the motion for the vibrating system in the micro-speaker as in Eq. 4, it should be noted that the matrix sizes in Eq. 4 are inevitably large as results of large number of nodes needed to precisely describe the complicated geometry of the corrugated diaphragm. It is well known that large number of nodes pose serious computation burden in performing dynamic

Table 3 Material properties of the diaphragm and VCM in the micro-speaker

Components	Properties		
	Young's modulus (N/m^2)	Poisson's ratio	Density (kg/m^3)
Diaphragm	8.08×10^9	0.25	1,360
VCM	7×10^{10}	0.3	2,582.9

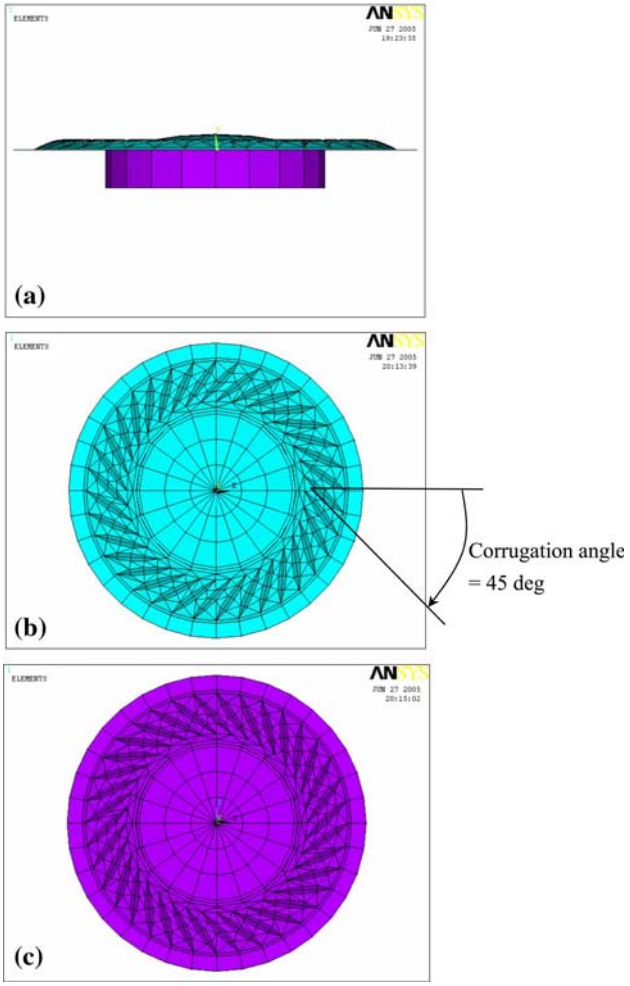

Fig. 5 The FEM model of the vibration system of the micro-speaker, including diaphragm and VCM. **a** Side view, **b** top view, **c** bottom view

simulation and/or analysis on the vibrating system. To solve the problem, the modal transformation analysis (Rao 1990) is employed to reduce the sizes of the matrices by first transforming the dynamics of the system into those in modal space and then considering only the first few modes to 20 kHz, the upper limit of human audibility. In this way, the associated computation burden is acceptable for a usual personal computer. The modal transformation starts with solving the generalized eigenvalue problem as

$$\mathbf{K}\mathbf{u}_\mathbf{r} = \omega_r^2 \mathbf{M}\mathbf{u}_\mathbf{r}, \tag{7}$$

where $\omega^2{}_r$ and $\mathbf{u_r}$ are the generalized eigenvalue and eigenvector, respectively, associated with the rth mode to be solved based on Eq. 7. The solved $\omega^2{}_r$ and $\mathbf{u_r}$ can be assembled in the matrix forms of

$$\mathbf{U} = [\mathbf{u_1} \quad \mathbf{u}_2 \quad \cdots \quad \mathbf{u_n}], \tag{8}$$

$$\Omega = \begin{bmatrix} \omega_1^2 & 0 & \cdots & 0 \\ 0 & \omega_2^2 & \cdots & 0 \\ 0 & 0 & \ddots & 0 \\ 0 & 0 & \cdots & \omega_n^2 \end{bmatrix}, \tag{9}$$

where $\mathbf{U}$ is called the modal matrix and $\mathbf{\Omega}$ is the frequency matrix with diagonals being the square of eigenvalues, i.e., ω_r's (in fact, natural frequencies). The modal transformation could be accomplished by

$$\mathbf{y} = \mathbf{U}\boldsymbol{\eta}, \tag{10}$$

where $\boldsymbol{\eta}$ contains the new system modal coordinates. Utilizing the transformation Eq. 10, the system equations Eq. 4 can be transformed into

$$\ddot{\boldsymbol{\eta}} + \alpha\dot{\boldsymbol{\eta}} + \Omega\boldsymbol{\eta} = \mathbf{U}^\mathrm{T}\mathbf{f}. \tag{11}$$

With the modal equations for the corrugated diaphragm derived in the above, the frequency response of the vibrating diaphragm can be well predicted. Knowing that fact that the human audibility is up to 20 kH, one can only consider the first m dominant modes represented by the first m equations in Eq. 11 and natural frequencies ω_i, $1 \le i \le m$, to predict the diaphragm dynamics. The new m dominant modal equations constitute so-called ''truncated model''. This model is prescribed m decoupled equations, significantly lessening the computation burden.

Combining the electromagnetic and mechanical models established, respectively, in Sects. 2.1 and 2.2, the vibrations of the corrugated diaphragm attached with a VCM subjected to an applied voltage can be predicted. This is accomplished by simply assembling Eqs. 11 and 3 with expression Eq. 1, resulting in

$$\ddot{\boldsymbol{\eta}} + \alpha\dot{\boldsymbol{\eta}} + \Omega\boldsymbol{\eta} = \frac{lI}{N_\mathrm{coil}}\mathbf{b}^\mathrm{T}\mathbf{y}_\mathrm{v,avg}\mathbf{U}^\mathrm{T}\mathbf{v}_\mathrm{cp}, \tag{12}$$

$$V = RI + L\frac{\mathrm{d}I}{\mathrm{d}t} + l\mathbf{b}^\mathrm{T}\mathbf{y}_\mathrm{v,avg}\frac{\mathbf{v}_\mathrm{cp}^\mathrm{T}\mathbf{U}\dot{\boldsymbol{\eta}}}{N_\mathrm{coil}}, \tag{13}$$

where N_coil the number of the interfacial nodes between the diaphragm and the attached VCM (where the axial Lorentz force generated by the coils acts); $\mathbf{v}_\mathrm{cp}$ is the position identification vector of the aforementioned nodes; $\mathbf{b} = [a_4, \ a_3, \ a_2, \ a_1, \ a_0]^\mathrm{T}$ is a vector containing polynomial coefficients in Eq. 2; $\mathbf{y}_\mathrm{v,avg}$ contains the axial displacements of the interfacial nodes between the vibrating diaphragm and the attached VCM, which is in fact

$$\mathbf{y}_{\mathrm{v,avg}} = \left[\left(\frac{\mathbf{v}_{\mathrm{cp}}^{\mathrm{T}}\mathbf{U}\boldsymbol{\eta}}{N_{\mathrm{coil}}}\right)^4 \quad \left(\frac{\mathbf{v}_{\mathrm{cp}}^{\mathrm{T}}\mathbf{U}\boldsymbol{\eta}}{N_{\mathrm{coil}}}\right)^3 \quad \left(\frac{\mathbf{v}_{\mathrm{cp}}^{\mathrm{T}}\mathbf{U}\boldsymbol{\eta}}{N_{\mathrm{coil}}}\right)^2 \quad \left(\frac{\mathbf{v}_{\mathrm{cp}}^{\mathrm{T}}\mathbf{U}\boldsymbol{\eta}}{N_{\mathrm{coil}}}\right) \quad 1 \right]^{\mathrm{T}}. \tag{14}$$

Note that the with the assumption that the whole diaphragm does not tilt while vibrating, the factor of the last term at the right hand side of Eq. 14, $\left(\frac{\mathbf{v}_{\mathrm{cp}}^{\mathrm{T}}\mathbf{U}\boldsymbol{\eta}}{N_{\mathrm{coil}}}\right)$, captures well the axial velocities of the interfacial nodes between the diaphragm and the VCM.

2.3 Acoustical modeling

It is aimed in this section to derive the sound pressure level (SPL) of the micro-speaker in audible frequency range, prior to which acoustic effect of the air on the vibrating membrane based on the theory of radiation mass is approximated, and also the vents of the outer case via the effective mass.

2.3.1 Radiation mass

When the diaphragm of the micro-speaker vibrates in the air, the presence of the air fluid loading near the surface of the diaphragm induces the effects of so-called radiation impedance in the form of

$$Z_{\mathrm{rad}} = R_{\mathrm{rad}} + jX_{\mathrm{rad}}, \tag{15}$$

where Z_{rad}, R_{rad}, and X_{rad} represent the radiation impedance, resistance and reactance, respectively. Due to the fact that the impedance normally affects only the high-frequency response of the vibration system, one can only consider the radiation reactance in Eq. 27. In this case, the radiation reactance can well approximated by

$$X_{\mathrm{rad}} = \pi a^2 \rho c X_1(2\,ka), \tag{16}$$

where a is the radius of the effective area of the diaphragm; ρ is density of the air; c is sound velocity; $k = 2\pi\ f/c$ is the wave number with f being the frequency; and

$$X_1(x) = \frac{2H_1(x)}{x} = \frac{4}{\pi}\left[\frac{x}{3} - \frac{x^3}{3^2 \times 5} + \frac{x^5}{3^2 \times 5^2 \times 7} - \cdots\right]. \tag{17}$$

$H_1\ (x)$ in Eq. 17 is called the Struve function of the first kind, where x is, for this study, the axial displacement of the vibrating diaphragm as the diaphragm is treated point vibrating source. In the FEM analysis, x is taken to be averaged axial displacement of the interfacial nodes between the diaphragm and the VCM; i.e., $x = \mathbf{b}^{\mathbf{T}}\,\mathbf{y}_{\mathbf{v,avg}}$. With X_{rad} calculated by Eq. 17, the radiation reactance can be captured by the following, which varies with the exciting frequency f,

$$m_{\mathrm{rad}} = \frac{X_{\mathrm{rad}}}{f}. \tag{18}$$

To add the above-obtained radiation mass to the interfacial nodes between the diaphragm and VCM, m_{rad} is further divided by the total number of interfacial nodes, N_{coils}, to be attached to the nodes as concentrated masses.

2.3.2 Effective mass of the vents

As illustrated by Fig. 1b, there are vents and a back chamber under the vibrating diaphragm in the micro-speaker. Based on the acoustic theories in (Kinsler 1982), they can be modeled integrally as a Helmholtz resonator, in which the air in the back chamber and vents is treated as acoustic compliance and inertance, respectively. Due to the fact that air inertia primarily affects the high-frequency response of the micro-speaker, only the acoustic inertance induced by the vents are included into the established FEM model. The acoustic inertance of vents can be captured by

$$I_{\mathrm{a}} = \frac{\rho l_{\mathrm{e}}}{S_{\mathrm{vent}}} \tag{19}$$

where l_{e} and S_{vent} are the effective length and cross-section area of the vents. Based on well-known the analogies between mechanical and acoustical systems as shown in Table 4, the effective mass due to the acoustic inertance can be approximated via multiplying the inertance by the cross-section area of the vents again, yielding

$$I_{\mathrm{a,m}} = \rho l_{\mathrm{e}} S_{\mathrm{vent}}. \tag{20}$$

Similar to the procedure of adding the radiation mass to the FEM model as stated in the previous subsection,

Table 4 Analogies between mechanical and acoustical systems

Mechanical system	Acoustical system
Velocity (m/s)	Flow (m^3/s)
Force (N)	Pressure (N/m^2)
Damping (kg/s)	Acoustic resistance (kg/s· m^4)
Mass (kg)	Acoustic inertance (kg/m^4)
Compliance = 1/stiffness (s^2/kg)	Acoustic compliance (m^4 s^2/kg)

the effective mass obtained by Eq. 20 is divided by total number of the interfacial nodes between the VCM and the diaphragm first and then added to the nodes as concentrated masses on back surface of the vibrating diaphragm.

With the modelings on electromagnetic/mechanical subsystems and the air surrounding the diaphragm and in the vents, the motion of the vibrating diaphragm can be predicted by solving Eqs. 12 and 13. The solved diaphragm motions is initially in the modal coordinates based on the solution procedure proposed. It should be noted that the inverse modal transformation should be further applied to render diaphragm motions in physical coordinates.

2.3.3 Sound pressure level (SPL)

Assuming the propagation of an acoustic wave radiated by the micro-speaker is in a homogeneous non-viscous fluid medium, the propagation is then governed by a linear wave equation

$$\nabla^2 p = \frac{1}{c^2}\frac{\partial^2 p}{\partial t^2}, \tag{21}$$

where p and c are acoustic sound pressure and sound speed, respectively. Based on Eq. 21, it can be derived that the sound power radiated by a microspeaker diaphragm vibrating in a mean rms surface velocity; i.e., $\langle \dot{y}_v^2(f) \rangle$, can be calculated by

$$W_{\text{rad}}(f) = \rho c S_{\text{rad}} \sigma(f) \langle \dot{y}_v^2(f) \rangle, \tag{22}$$

where S_{rad} and σ are the effective cross-section area of the diaphragm and radiation efficiency, respectively. The surface velocity $\dot{y}_v$ in the term of $\langle \dot{y}_v^2(f) \rangle$ in Eq. 22 can be obtained by averaging axial velocities at the interfacial nodes between the diaphragm and VCM. The sound radiation efficiency σ can be calculated by a simplified equation Eq. 16

$$\sigma(f) = \frac{k^2 a^2}{1 + k^2 a^2}, \tag{23}$$

assuming the diaphragm as a monopole source. In Eq. 23, as defined previously, $k = 2\pi f/c$ is the wave number and a is the diaphragm radius. Note that based on Eq. 22 the radiation sound power provided by the micro-speaker depend on the driving frequency, since σ and $\langle \dot{y}_v^2(f) \rangle$ are frequency-dependent. With the radiation power in hand, the sound power level of the micro-speaker can be calculated by

$$L_{\text{w}} = 10 \log_{10}\left(\frac{W_{\text{rad}}}{W_{\text{ref}}}\right), \tag{24}$$

where W_{ref} represents the reference sound power of 10^{-12} W. The micro-speaker would be measured in the anechoic chamber without other sound sources and placed on a hard baffle. At a distance of d meter from the micro-speaker with sound power W_{rad} watts, the sound intensity is

$$I_{\text{rad}} = \frac{W_{\text{rad}}}{2\pi d^2} \tag{25}$$

for radiating spherical wave. The sound intensity can also described as the form with sound pressure

$$I_{\text{rad}} = \frac{p_{\text{rms}}^2}{\rho c}, \tag{26}$$

where p_{rms} denotes root-mean-square pressure from the source. Combining Eqs. 25 and 26 leads to

$$p_{\text{rms}}^2 = \frac{W_{\text{rad}} \rho c}{2\pi d^2}, \tag{27}$$

On the other hand, the definition of the sound pressure level (SPL) is

$$L_{\text{p}} = 10 \log_{10}\left(\frac{p_{\text{rms}}^2}{p_{\text{ref}}^2}\right), \tag{28}$$

where p_{ref} is the reference sound pressure of 2×10^{-5} Pa. Incorporating Eq. 27 into Eq. 28, the SPL could be stated as

$$L_{\text{p}} = 10 \log_{10}\left(\frac{W_{\text{rad}} \rho c}{2\pi d^2 p_{\text{ref}}^2}\right), \tag{29}$$

and then

$$L_{\text{p}} = 10 \log_{10}\left(\frac{W_{\text{rad}}}{W_{\text{ref}}}\right) - 20 \log_{10}(d) + 10 \log_{10}\left(\frac{W_{\text{ref}} \rho c}{2\pi p_{\text{ref}}^2}\right). \tag{30}$$

The first term in Eq. 30 is known as sound power level of the source which is given in Eq. 22 and the other two terms depends on constant parameters. It should be noted that the sound velocity and density of the air are treated as 343.4 m/s and 1.204 kg/m^3, respectively, when the room temperature is 20°C. Subsequently, the SPL expression in Eq. 30 can be obtained by

$$L_{\text{p}} = L_{\text{w}} - 20 \log_{10}(d) - 7.8194. \tag{31}$$

With Eq. 31 in hand, where L_w needs to be calculated based on the diaphragm motions solved by Eqs. 12 and 13, the frequency response of a micro-speaker in SPL can be calculated to evaluate its acoustic performance. The flow chart in Fig. 6 depicts the whole solution/analysis procedure to obtain the frequency response of a micro-speaker in terms of SPL. It can be seen from this chart that nonlinearities arise mainly from uneven magnetic flux intensity distribution and back EMF.

3 Simulation results

Simulations are conducted to understand dynamic and acoustic insights of the considered micro-speaker. The material properties of the diaphragm and the VCM for the micro-speaker shown in Fig. 2 are given Table 3, which would be used in simulations herein and later experiments. On the other hand, Table 5 lists the experimentally identified electrical properties of the VCM in the speaker. Following the computation procedure proposed in Sect. 2 and illustrated by a block diagram in Fig. 6, the dynamic and acoustic performances of the micro-speaker can be fully captured. As carrying out the computations, three different models with varied acoustic assumptions are considered to investigate the effectiveness of the various models. The

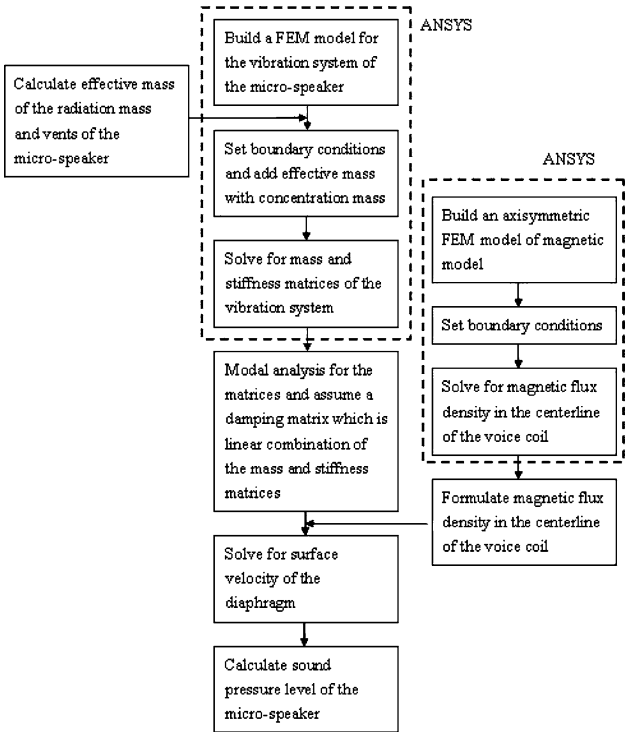

Fig. 6 The analysis procedure in a block diagram

Table 5 Identified electrical parameters of the VCM

Voltage (V)	2.828 (Volt)
Resistance (R)	8 (Ω)
Inductance (L)	2×10^{-4} (H)
Length of Coils (l)	0.78 (m)

first model is without considering effects of radiation mass induced by the air and effective mass by the vents. The second model considers only effects of radiation mass of the air. The third one takes into account both radiation mass by the air and the effective mass by the vents.

Figure 7 shows the calculated magnitudes of the averaged normal (axial) velocities of the diaphragm; i.e., $|\dot{y}_v|$, across diaphragm area with respect to a swept sine for three different acoustic assumptions. The diaphragm considered herein has baseline 45° corrugation. Two peaks can be found for the responses based on three different models. The first peaks are at about 900 Hz and the second peaks around 10,000 Hz in slight difference from model to model. The frequency locations for the aforementioned peaks in fact coincide with the first and second natural frequencies of the thoertical established in the form of Eq. 4, i.e., ω_1 and ω_2 defined in Eq. 9, proving that the large velocity responses appearing in Fig. 7 arises from resonance. It is also noted from the figure that no large variation in the resonances due to different acoustic assumptions is observed, while the level of diaphragm velocity is raised moderately with addition of radiation mass of the air and the effective mass of the vents. This

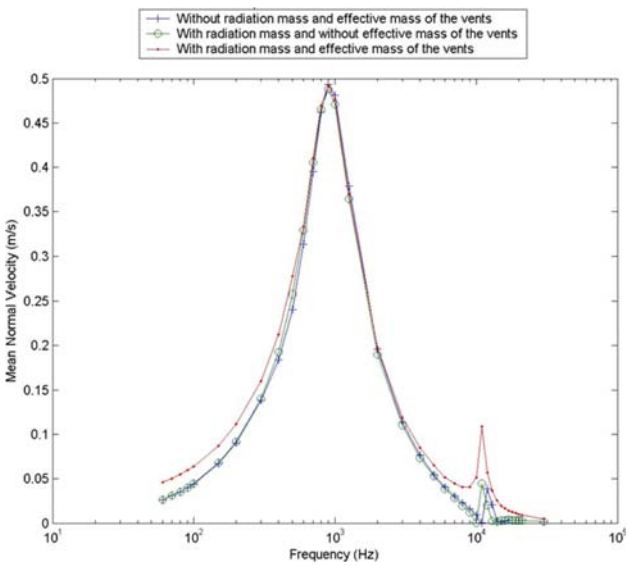

Fig. 7 Mean normal velocities of the diaphragm as opposed to varied driving frequency

increase should enhance the sensitivities of the microspeaker in SPL. The associated VCM currents computed by the same procedure are shown in Fig. 8, where it seen that as the vibrating frequency of the diaphragm increases, the current decrease significantly above 1,000 Hz. This is largely due to a significant increase in the back EMF term in Eq. 3. On the hand, the VCM impedance is also computed and shown in Fig. 9, where it is seen that as the vibrating frequency increases, the impedance increases significantly above 1,000 Hz, also due to the larger back EMF term in Eq. 3 in the range of higher frequencies. Finally, the driving Lorentz force induced by the electromagnetic interaction between the VCM and the imposed magnetic field is computed and shown in Fig. 10. A clear

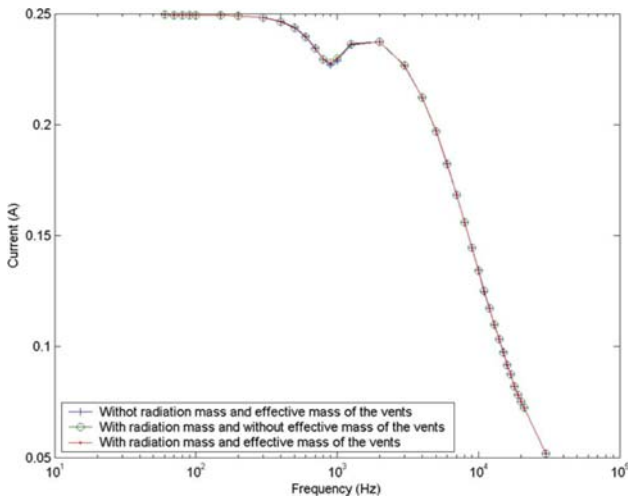

Fig. 8 The current in VCM as opposed to varied driving frequency

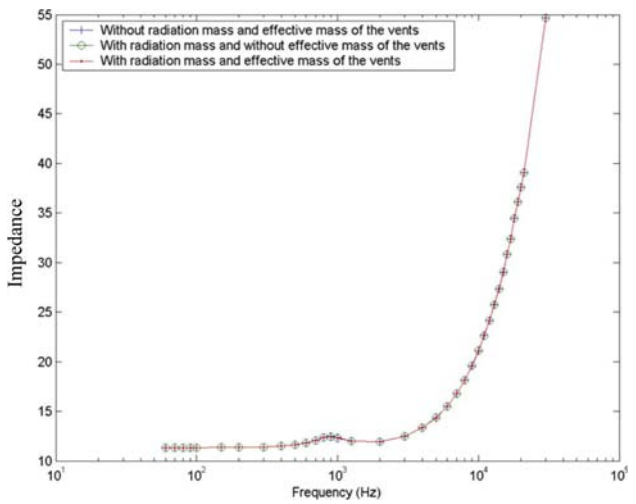

Fig. 9 The impedance of the VCM as opposed to varied driving frequency

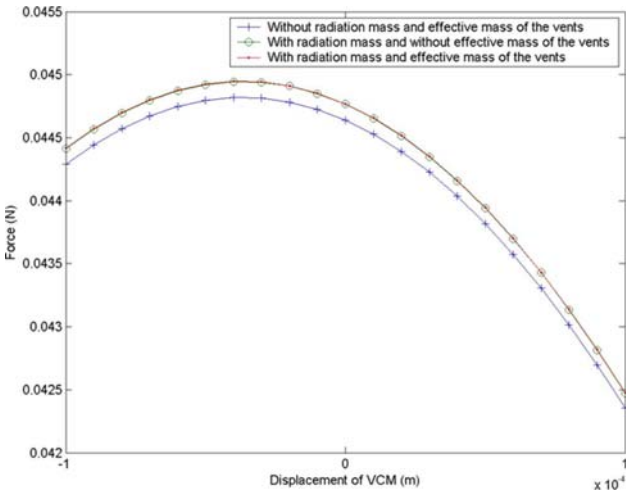

Fig. 10 The Lorentz force generated by the VCM as opposed to the normalized position of the VCM's axial position with driving frequency of 900 Hz

nonlinearity of the force as opposed to the instantaneous vibrating position of the diaphragm in the axial direction is present in this figure. This primarily results from uneven magnetic flux intensity distribution. Furthermore, the model with addition of radiation mass of the air and the effective mass of the vents renders smaller force leads to smaller driving force. This is due to the fact that the nominal, equilibrium axial position of the VCM coils is lower for the model with two mass effects than those for the others because of gravity; thus, in the normalized vibrating range of the VCM coils shown in Fig. 10 for the model considering two masses, the VCM experiences different distribution of magnetic flux intensity than others.

With the diaphragm velocity calculated as shown in Fig. 7, the sound pressure level (SPL) of the microspeaker is ready to be computed for performance evaluation, using Eqs. 22–24 and 31. The computed SPLs for different acoustic assumptions and corrugation angles are shown, respectively, in Figs. 11 and 12. The different corrugation angles considered are 15°, 45°, 75°. It is seen from Fig. 11 that three different models renders similar SPLs up to the mid-range of the audible frequencies, around 4 kHz. However, the one considering both radiation mass of the air and the effective mass of the vents has larger SPLs as the frequency is above 4 kHz and up to 20 kHz, the upper limit of human audibility. Another difference of the case with both masses considered from the other two simpler cases are the absence of anti-resonances at approximate 900 and 10.8 kHz. This is due to the combined damping effect induced by both radiation and effective masses. Also depicted in Fig. 11 are the

SPLs without diaphragm corrugation and selected mode shapes at approximate 900, 1.1 and 10.1 kHz. The SPLs without corrugation appears to have smaller response than the ones considering air mass below the first resonances, while owns much strong first resonance. It appears that the diaphragm with corrugation leads to a flatter SPL curve than that without, proving the well-known merit of the corrugation—lessening sound distortion. It is also seen that both mode shapes of Modes 1 and 6 are axisymmetric, the resonances of which appear to impact the dynamic characteristics of the micro-speaker more significantly than other. This is due to the reason that unaxisymmetric modes tend to cancel almost all normal velocities such as the second mode shape presented in Fig. 11; thus, only mode shapes which are axisymmetry contribute to have peaks in the SPL responses. On the other hand, it is seen from Fig. 12 that the SPLs for all corrugation angles are close to each other, while the one with 45° has generally highest SPLs across all frequencies.

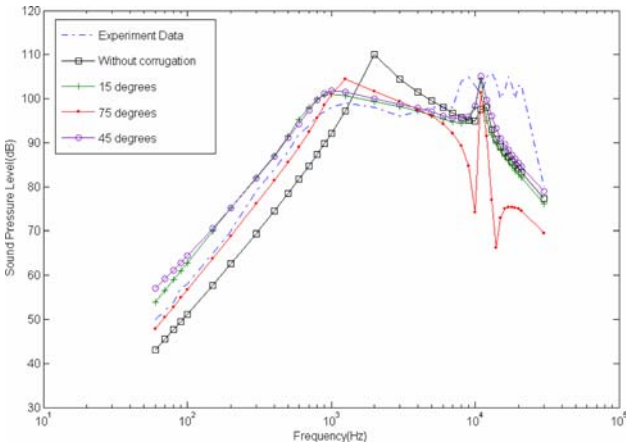

Fig. 12 The simulation results with varied corrugation angles of the diaphragm and associated experimental data

4 Experimental validation

Also shown in the Figs. 11 and 12 are the SPLs measured by an experiment system, which is set up in a laboratory. With measured SPLs, the models established in Sect. 3 for predicting the micro-speaker performance and effects of corrugation angles can be validated and explored, respectively. The experimental setup, as schematically illustrated in Fig. 13, consists of a microphone to measure the sound pressure generated by the micro-speaker, a Sunlight 1,600 series Electro-acoustics Analyzer to acquire the measurements and converted them to SPLs, and a baffle screen to fix the measuring microphone. The measurement process starts first with mounting the micro-speaker on the baffle in a distance of 5 cm from the microphone. Having applied voltage to VCM of the speaker, the SPL responses of the micro-speaker are then be acquired by the microphone and processed by the analyzer. All experimental components except for the analyzer are placed in a anechoic chamber, which provides an environment nearly without sound reflection, then resulting in an extremely low background sound noise and vibration.

The experimentally measured SPLs are shown both in Figs. 11 and 12 for comparison with theoretical simulations in solid curves. It can be seen from Fig. 11 that a general closeness is present between the theoretical response with diaphragm corrugation and the

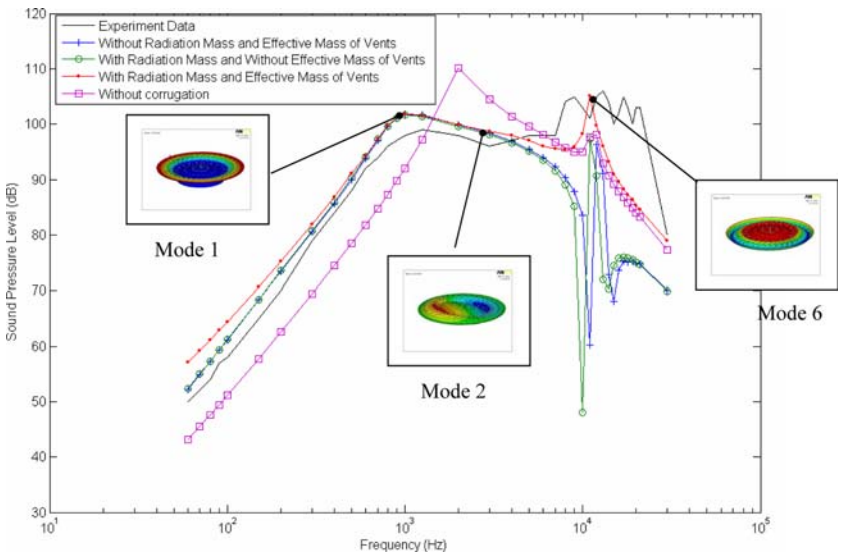

Fig. 11 The simulation results under varied acoustic assumptions and experimental data of the micro-speaker

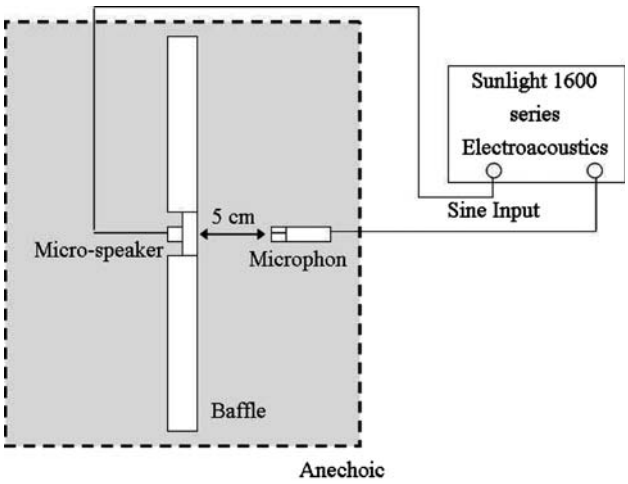

Fig. 13 The experimental setup for measuring sound pressure level of the micro-speaker

experimental counterparts up to the mid-frequency of 4 kHz, indicating adequate validity of the theoretical model established. However, obvious discrepancy appears above 4 kHz, which, based on basic theory of a speaker, should be due to the lack of considering air enclosure above and below the vibrating diaphragm in the structure of the micro-speaker as shown in Fig. 1. The consideration should lead to stronger responses above 4 kHz for theoretically-predicted SPLs. On the other hand, it is also seen from this figure for the experimental data alone that five peaks are present. The closeness is present between the frequencies corresponding to the first and second peaks of the experimental curve (around 1 and 10.2 kHz, respectively), and the first and second theoretical resonances of the first and sixth modes obtained by the previous FEM and modal analysis in Sect. 2, showing another sign of validity for the theoretical model. Other experimental peaks are seen located between high frequencies from 9,000 to 21,000 Hz, which cannot precisely be predicted by any theoretical model established in this study. This modeling insufficiency is again due to the lack of considering air enclosures above and below the vibrating diaphragm. Finally, it is seen from Fig. 12 that the response with corrugation angle of 45° is very close to the experimental data for the realistic speaker with also 45° corrugation, validating in another way the effectiveness of the theoretical model established in this study.

5 Conclusions and future works

An effective micro-speaker model is successfully established in this study via the analysis on electromagnetic, mechanical, and acoustical subsystems. The model takes into particular account the nonlinearities arisen from an uneven magnetic flux intensity distribution and back EMF, and diaphragm corrugations in varied angles. For acoustic analysis, three different models with or without radiation mass and effective mass of the vents are considered. Assembling all subsystems, the net equations of motion can be obtained. Simulations are next conducted to explore micro-speaker dynamics, along with which experimental study is conducted to verify the effectives of the theoretical models. Based on the theoretical and experimental results, the following conclusions can be drawn:

(1) Simulations show that the diaphragm with corrugation leads to a flatter SPL curve than that without, proving the well-known merit of the corrugation—lessening sound distortion.
(2) The established models are capable of predicting the SPL response of the micro-speaker up to the mid-frequency of 4 kHz, indicating some level of validity for the theoretical model established.
(3) In the frequency range above 4 kHz, theoretical SPL responses deviates from the experimental counterparts. This is due to the lack of considering air enclosure above and below the vibrating diaphragm in the structure of the micro-speaker.
(4) The simulated response with corrugation angle of 45° is most close among all angles to the experimental data for the realistic speaker with also 45° corrugation, validating in another way the effectiveness of the theoretical model established in this study.

To minimize the discrepancy between theoretical and experimental responses of the micro-speaker at high frequencies, efforts should be paid in the future to perform modeling on the air enclosure above and below the diaphragm in the structure of the speaker.

Acknowledgements The authors would like to pay special thanks to National Science Council of Republic of China for financially supporting this research project through the supporting contracts with nos. NSC 94-2622-E-033-011-CC3, 94-2212-E-033-010, 94-2745-E-033-004-URD, and also to the Center-of-Excellence Program on Membrane Technology, the Ministry of Education, Taiwan, ROC.

References

Al-Ali KM, Packard AK, Tongue BH (2000) Lumped-parameter Modeling of Vented-box Loudspeakers. In: Proceedings of the American control conference 5:3023–3027

Beranek LL (1954) Noise and vibration control. McGraw-Hill, New York

Hwang GY, Kim KT, Chung SU, Hwang SM, Kang BS (2002a) Analysis of a dynamic speaker in a mobile phones by considering mechanical, electrical, and magnetic coupling effects. J Appl Phys 91(10):6979–6981

Hwang GY, Kim HG, Hwang SM, Kang BS (2002b) Analysis of harmonic distortion due to uneven magnetic field in a microspeaker used for mobile phones. IEEE Trans Magn 38(5):2376–2378

Hwang SM, Hwang GY, Kwon JH, Lee HJ, Hang BS (2003a) Performance comparison between circular and elliptical type microspeakers for cellular phones. IEEE Trans Magn 39(5):3256–3258

Hwang GY, Lee HJ, Hwang SM, Kang BS, Jeung SK (2003b) Performance comparison between inner and outer permanent magnet type microspeakers used for mobile phones. J Appl Phys 93(10):8519–8521

Kaizer AJM (1987) Modeling of the nonlinear response of an electrodynamic loudspeaker by a volterra series expansion. J Audio Eng Soc 35(6):421–433

Kinsler LE (1982) Fundamentals of acoustics. Wiley, New York

Kippel W (1990) Dynamic measurement and interpretation of the nonlinear parameters of electrodynamic loudspeakers. J Audio Eng Soc 38(12):944–955

Kippel W (1992) Nonlinear large-signal behavior of electrodynamic loudspeakers at low frequenicies. J Audio Eng Soc 40(6):483–496

Novak JF(1959) Performance of enclosures for low resonance high comliance loudpsekers. J Audio Eng Soc 7(1):29–37

Rao SS (1990) Mechanical vibrations. Wiley, California

Small RH (1972) Direct radiator loudspeaker system analysis. J Audio Eng Soc 20(5):383–95

Small RH (1972) Closed-box loudspeaker systems-part 1: analysis. J Audio Eng Soc 20(10):798–808

Tappan PW (1959) Analysis of a low-frequency loudspeaker system. J Audio Eng Soc 7(1):38–46